Published in final edited form as:
Exp Eye Res. 2014 August ; 125: 95–106. doi:10.1016/j.exer.2014.06.005.

Insulin treatment normalizes retinal neuroinflammation but not markers of synapse loss in diabetic rats

Dustin R. Masser[a,b,c,†], **Heather D. VanGuilder Starkey**[a,d,†], **Georgina V. Bixler**[a], **Wendy Dunton**[e], **Sarah K. Bronson**[d,e], and **Willard M. Freeman**[a,b,c,d,*]

Dustin R. Masser: dmasser@ouhsc.edu; Heather D. VanGuilder Starkey: hdv108@psu.edu; Georgina V. Bixler: gbixler2@hmc.psu.edu; Wendy Dunton: wgd7n@virginia.edu; Sarah K. Bronson: sbronson@hmc.psu.edu

[a]Department of Pharmacology, 500 University Drive, Penn State College of Medicine, Hershey PA 17033 USA

[b]Department of Physiology, BMSB 653, P.O. Box 26901, Oklahoma University Health Sciences Center, Oklahoma City OK 73216 USA

[c]Reynolds Oklahoma Center on Aging, SLY-BRC 1370, 975 NE 10[th]St, Oklahoma City OK 73104 USA

[d]Penn State Hershey Eye Center, 500 University Drive, Penn State College of Medicine, Hershey PA 17033 USA

[e]Department of Cellular and Molecular Physiology, 500 University Drive, Penn State College of Medicine, Hershey PA 17033 USA

Abstract

Diabetic retinopathy is one of the leading causes of blindness in developed countries, and a majority of patients with type I and type II diabetes will develop some degree of vision loss despite blood glucose control regimens. The effects of different insulin therapy regimens on early metabolic, inflammatory and neuronal retinal disease processes such as retinal neuroinflammation and synapse loss have not been extensively investigated. This study compared 3 months non-diabetic and streptozotocin (STZ)-induced diabetic Sprague Dawley rats. Diabetic rats received either no insulin treatment, systemic insulin treatment beginning after 1 week uncontrolled diabetes (early intervention, 11 weeks on insulin), or after 1.5 months uncontrolled diabetes (late intervention, 6 weeks on insulin). Changes in both whole animal metabolic and retinal inflammatory markers were prevented by early initiation of insulin treatment. These metabolic and

*Corresponding author: Willard M. Freeman, BMSB 653, P.O. Box 26901, Oklahoma University Health Sciences Center, Oklahoma City OK 73216 USA; 01-405-271-8000 ext. 30729; wfreeman@ouhsc.edu.
†These authors contributed equally to the report

Author Contributions:
HDS, SKB and WMF designed experiments. HDS and GVB carried out all experiments. WD generated and maintained animal cohorts with the supervision of SKB. DRM, HDS, SKB and WMF analyzed and interpreted all data. DRM, HDS, and WMF prepared the manuscript. All authors have read and approved the manuscript. All the authors declare no conflicts of interest.

inflammatory changes were also normalized by the later insulin intervention. Insulin treatment begun 1 week after diabetes induction ameliorated loss of retinal synapse markers. Synapse markers and presumably synapse numbers were equivalent in uncontrolled diabetes and when insulin treatment began at 1.5 months of diabetes. These findings are in agreement with previous demonstrations that retinal synapses are lost within 1 month of uncontrolled diabetes and suggest that synapses are not regained with glycemic control and restoration of insulin signaling. However, increased expression of metabolic and inflammatory markers associated with diabetes was reversed in both groups of insulin treatment. This study also emphasizes the need for insulin treatment groups in diabetic retinopathy studies to provide a more faithful modeling of the human condition.

Keywords

Diabetes; retina; synapse; neuroinflammation; insulin; metabolic memory

1. Introduction

Diabetic retinopathy (DR) is a neurovascular disease secondary to metabolic dysregulation and loss of insulin signaling with diabetes. It remains the leading cause of blindness in developed countries among working age adults. Both type I and type II diabetic patients are at risk for developing DR and the majority of diabetics will develop some degree of vision loss (Antonetti et al., 2006; Antonetti et al., 2012; Intine and Sarras, 2012). The pathobiological sequelae of DR are still not fully determined; however extensive data provide evidence for a multifactorial disease arising from inflammatory, neuronal and vascular deficits in the retina in response to metabolic dysregulation with diabetes (Antonetti et al., 2006). Recent findings have established that DR can be considered a disease of the retinal neurovascular unit (Antonetti et al., 2012). Additionally, studies suggest the neuronal deficits in DR occur prior to the overt, clinically identifiable vascular complications (Barber et al., 2005; Barber et al., 1998; Jackson and Barber, 2010; VanGuilder et al., 2008). Similarly, induction of systemic inflammation and local inflammation of the retina has been implicated in the early disease process (Kastelan et al., 2013; Pietropaolo et al., 2007; Rungger-Brandle et al., 2000). Local retinal neuroinflammation occurs in DR as a result, in part, of the breakdown of the blood retinal barrier (Antonetti et al., 2006). Immunostimulating proteins from the systemic inflammation, as well as direct effects of excess glucose on resident glial cells, contribute to a pro-inflammatory state (Antonetti et al., 2012; Tang and Kern, 2011). Neuronal deficits associated with DR are attributed to a combination of neuronal apoptosis and loss of retinal synapses (Barber et al., 2011; VanGuilder et al., 2008). Microvascular proliferation, as well as occlusions and vessel hemorrhaging, occur in late stage disease processes, resulting in the most overt clinical signs of proliferative DR and have been the primary target of therapeutic development (Antonetti et al., 2012).

Analogs of these clinical aspects of DR progression are also evident in animal models. Vascular defects occur in a variety of animal models of DR, but the vascular proliferation indicative of advanced clinical DR is typically not found in animal models (Lai and Lo,

2013). Neuronal deficits in retinal ganglion cells and amacrine cells including dysfunction, apoptosis, and synapse loss have been shown in multiple animal models of DR (Gastinger et al., 2006; Kern and Barber, 2008). Similarly, inflammation and inflammatory markers are present in retinas of DR animal models (Gaucher et al., 2007; Yang et al., 2009; Zorena et al., 2013). The retinal neuronal and inflammatory changes are postulated to precede vascular dysfunction in experimental diabetes (Aung et al., 2013; Fernandez et al., 2012). While the sequence of vascular, neuronal, and inflammatory events in early DR progression is not fully understood, it is likely that these processes are inter-related (Antonetti et al., 2006). Multiple studies have investigated the time course of individual inflammatory, vascular or neuronal events; however, the effects of long-term insulin replacement across these early disease processes have not been extensively studied. The role of insulin treatment in disease progression is clinically relevant not only because nearly all type I, and many type II diabetic patients receive insulin replacement, but because of the growing understanding that periods of poor glycemic control may contribute to complication development through metabolic memory (Pirola et al., 2010; Zhang et al., 2012). Clinical and animal model studies demonstrate the metabolic memory phenomenon whereby a period of poor glycemic control continues to confer a higher disease risk even after establishment of good glycemic control (Aiello and DCCT/EDIC Research Group, 2014; Engerman and Kern, 1987; Intine and Sarras, 2012; Pirola et al., 2010). Moreover, to understand early disease processes and eventually develop DR preventative therapies, a background of exogenous systemic blood glucose control is needed in preclinical studies to model the human condition and the accepted standard of care.

This study sought to examine whether specific measures of whole animal physiology, retinal neuroinflammation and synaptic maintenance demonstrate metabolic memory using a model that we have previously reported to demonstrate molecular changes consistent with the metabolic memory phenotype (Bixler et al., 2011; Brucklacher et al., 2008; Freeman et al., 2010).

2. Methods

2.1 Animals

All rats were housed in a specific pathogen-free Penn State Hershey Diabetic Complications Animal Barrier Facility for the duration of the study, and maintained in accordance with the Institutional Animal Care and Use Committee guidelines. Food (Teklad #2018 global 18% protein diet, irradiated; Harlan Laboratories, Madison, WI) and water were freely available throughout the study, unless otherwise stated. Two cohorts of male Sprague-Dawley rats were purchased at 100–125g body mass (Charles River, Wilmington, MA). After one week of quarantine, all rats were fasted overnight and diabetes was induced by intraperitoneal injection of 65mg/kg streptozotocin (STZ; Sigma Aldrich, St. Louis, MO) dissolved in 10mM sodium citrate (pH 4.5) as previously described (Bixler et al., 2011; VanGuilder et al., 2011). Non-diabetic (ND) control rats received the same treatment but were injected with an equal volume of citrate buffer. Induction of diabetes was confirmed one week following injection by blood glucose (BG) testing; only STZ-injected rats with blood glucose levels >250mg/dL were included in the study.

Diabetic rats received either no insulin (D) or insulin replacement delivered by subcutaneous implantation of insulin pellets (26mg, 7mm x 2mm; LinShin Canada, Scarborough, Canada) via trocar, under brief 70% CO_2/30% O_2 anesthesia. The diabetic/early intervention (D/EI) group received insulin replacement beginning one week following STZ injection, upon confirmation of hyperglycemia. The diabetic/late intervention (D/LI) group received insulin replacement beginning six weeks after diabetes-induction (Figure 1a). Insulin-treated rats received a second insulin implant when midday non-fasting BG exceeded 250mg/dL or when body weight exceeded 300g. BG and body mass were monitored throughout the experiment. Twelve weeks following diabetes induction, or citrate vehicle injection in the case of ND controls, all rats were sacrificed by decapitation under pentobarbital anesthesia (Nembutal, 100mg/kg; Ovation Pharmaceuticals Inc., Deerfield, IL) administered by a single intraperitoneal injection. Group and cohort information is presented in Table 1.

2.2 Body composition analysis

Whole-body composition of rats was characterized by time domain nuclear magnetic resonance (NMR). Briefly, anesthetized rats were placed in a proton NMR analyzer (Bruker LF90 proton-NMR Minispec, Bruker Optics, The Woodlands, TX), and fluid, lean, and fat tissue masses were assessed just prior to sacrifice. Percent fluid, lean, and fat masses were calculated based on total body mass.

2.3 Blood glucose analysis

Beginning one week following injection of STZ or citrate vehicle and subsequently weekly for insulin treated groups (D/EI and D/LI) or biweekly for ND and D groups throughout the 12-week timecourse, BG levels were assessed in a drop of blood from a tail nick (Lifescan One-touch Meter; Johnson & Johnson, Milpitas, CA) as previously described (Bixler et al., 2011).

2.4 Glycated hemoglobin analysis

At sacrifice, glycated hemoglobin (HbA1c) and total hemoglobin levels were measured in 1μL of blood from a tail nick using specific monoclonal antibody agglutination immunoassay cartridges and DCA analyzer (Bayer Diabetes Care, Whippany, NJ). Percent HbA1c was calculated as previously described (Bixler et al., 2011).

2.5 Ketone analysis

At sacrifice, ketone levels were measured in 1.5μL whole blood from a tail nick using an electrochemical blood ketone meter (Precision Xtra; Abbott Diabetes Care Inc., Alameda, CA) that quantifies the current generated by enzymatic conversion of beta hydroxybutyrate to acetoacetate and subsequent redox conversion of resulting NADH to NAD^+.

2.6 Branched-chain amino acid analysis

The concentration of branched-chain amino acids was quantified in serum prepared from trunk blood collected during sacrifice using the method previously described by Beckett (Beckett, 2000). Production of NADH by leucine dehydrogenase-mediated catalysis of

isoleucine, leucine, and valine was assessed spectrophotometrically at 340nm (Toyoba Labs, New York, NY).

2.7 Quantitation of c-peptide and insulin

Endogenous rat c-peptide and exogenous human insulin were quantified by enzyme-linked immunosorbent assays (Mercodia, Uppsala, Sweden) from plasma collected at sacrifice to assess endogenous and exogenous serum insulin levels. Ten μL of plasma was used in the rat c-peptide assay and 25μL was used in the human insulin assay.

2.8 RNA isolation and quantitative PCR

Whole retinas were homogenized in 500 μL TriReagent (Molecular Research Center, Cincinnati, OH) by bead mill (Retsch TissueLyzer II, Qiagen, Valencia, CA) using 3 mm stainless steel balls at 30 Hz for 30 seconds, as previously described (Bixler et al., 2011; Brucklacher et al., 2008). RNA was isolated from retinal homogenates using standard TriReagent/BCP disruption and phase separation. Following overnight precipitation by incubation with isopropanol at −20°C, RNA was purified using the Qiagen RNeasy Mini kit (Qiagen). Quantity and quality assessments were made by spectrometry (NanoDrop ND1000; Thermo Scientific, Wilmington, DE) and microfluidics chip (Agilent 2100 Expert Bioanalyzer Nano Chip, Agilent, Palo Alto, CA), respectively. Only samples with RNA integrity numbers >8 were used in analyses.

qPCR analysis of targets of interest (n=8 animals/group) was performed as previously described using TaqMan Assay-On-Demand (Applied Biosystems, Foster City, CA) gene-specific primers and probes and a 7900 HT Sequence Detection System (Applied Biosystems) (Bixler et al., 2011; Brucklacher et al., 2008). Relative gene expression was calculated with SDS 2.2.2 software using the $2^{-\Delta\Delta}$Ct analysis method with β-actin as an endogenous control. β-actin expression was determined to be unchanged between animal groups in a preliminary absolute quantitation experiment (data not shown). For a full list of primer/probe sets, see Table 2.

Heatmap, clustering, principal components analysis, and support vector machine analysis were conducted with GeneSpring GX 12.6 (Agilent). Relative mRNA quantitation (RQ) values were scaled to make the ND group mean equal to 1. Hierarchical clustering of samples for the heatmap was performed using Euclidean distance and complete linkage. K-means clustering was performed on conditions with a Manhattan similarity measure set for 4 clusters. Classification analysis by support vector machine used a linear kernel function with a ratio and sigma of 1. The classification model was built with data from ND and D groups with D/EI and D/LI rats subsequently classified as ND or D.

2.9 Immunohistochemistry

Detection of Iba1 and synaptophysin by immunohistochemistry (IHC) was carried out as described previously (VanGuilder et al., 2008). Briefly, whole eyes were enucleated immediately after sacrifice, embedded in Tissue-Tek OCT compound (SakuraFinetek, Torrance, CA, USA) and frozen with isopentane on dry ice. Ten-micrometer sections, generated from cryostat sectioning (HN 505E; Microm International, Walldorf, Germany),

were fixed at room temperature with 2.0% paraformaldehyde and blocked in 10% donkey serum (Jackson ImmunoResearch, West Grove, PA, USA) with 0.1% Triton X-100 in PBS. Primary antibody incubation (anti-Iba1: 01919741, Wako Richmond, VA, anti-synaptophysin: ab8049 Abcam, Cambridge, MA) was carried out in blocking solution overnight, and subsequently washed with 0.1% Triton X-100 in PBS. Sections were then incubated with secondary antibodies (Dylight 649: 711496152, Dylight 488: 715486150 Jackson ImmunoResearch) counterstained with Hoechst (5 μg/mL) and coverslipped in Aqua Poly/mount (Polysciences, Warrington, PA, USA).

Detection of glial fibrillary acidic protein (GFAP) was carried out on whole retinal flat mounts. Retinas were excised after sacrifice and rinsed twice with ice-cold PBS, fixed in 4% paraformaldehyde in PBS for 1 hour, rinsed three times in PBS at RT for 15 minutes, and mounted on glass slides by making four to five slits as needed with microdissection scissors with the ganglion cell layer facing up. IHC was then carried out as described above (anti-GFAP: ab7260 Abcam).

All IHC images were acquired with a Leica confocal laser scanning microscope (TCS SP2 AOBS, Exton, PA, USA), with a UV-diode laser for Hoechst (405 nm), an argon laser for Cy2 (488 nm) and helium–neon lasers for Cy3 and Cy5 (543 and 633 nm, respectively). Broad field images of regions of interest were acquired using 20x oil-immersion objective, while high-resolution targets were imaged with a 63× oil-immersion objective as a series of optical sections (0.3-μm step size, 1024 × 1024 pixels) using identical laser settings optimized on control sections and presented as maximum projections of 8.3 μm *z*-stacks. Brightness and contrast were optimized using Adobe Photoshop CS5 Extended 12.04 software (Adobe Systems Inc., San Jose, CA, USA). Comparative images within figures were acquired and adjusted with identical microscope and software settings.

To assess the density of synaptophysin-immunoreactive (SYP-IR) puncta in retinas sections (n =7–8 animals per group), three to four sections (z = 10 μm) per eye were processed. Two hundred and fifty-micrometer lengths of the inner and outer plexiform layers were imaged separately with a confocal laser scanning microscope (63× oil-immersion objective, 4× optical zoom), and rendered as maximum projections. With the analyst blinded to sample identity, the total number of SYP-IR puncta per section were determined using automated imaging analysis software (ImageJ with nucleus counter program plugin; NIH, Betheda, MD, USA). The resulting data were averaged per eye, standardized to average control values, and presented as percentage of control ± SEM.

2.10 Statistics

Endpoints were analyzed by One-Way ANOVA with Student-Newman-Keuls pairwise post-hoc testing with α=0.05. Gene expression data (ANOVA and Pearson Correlation) was corrected for multiple comparisons by the Benjamini Hochberg method (Benjamini et al., 2001).

3. Results

3.1 Blood Glucose and Body Weight Monitoring

Diabetic (D) groups demonstrated a rapid elevation of blood glucose (BG) to 500mg/dL following STZ induction. The Diabetic/Early Intervention (D/EI) group was implanted with insulin pellets 1 week after STZ induction and BG levels returned to levels equivalent to the Non-Diabetic (ND) controls (Figure 1b). BG levels increased slightly over the subsequent weeks until a replacement pellet was implanted at the 7 week timepoint. The Diabetic/Late Intervention (D/LI) group was consistently hyperglycemic until the implantation of insulin pellets at 6 weeks. Insulin-treatment group rats received an additional insulin implant when midday non-fasting BG exceeded 250mg/dL or when body weight exceeded 300g. At sacrifice, non-insulin treated D group rats were hyperglycemic compared to all other groups and BG levels of D/LI rats were slightly higher as compared to the ND and D/EI groups (Figure 1c).

Body weight was monitored throughout the study. During periods of hyperglycemia/ hypoinsulinemia, the D group did not gain weight as quickly as ND or insulin treated diabetic groups (Figure 1d). With insulin treatment, D/EI and D/LI animals gained weight at a similar rate to controls. At sacrifice, all diabetic groups were underweight as compared to ND and the D/LI group was lighter than D/EI rats (Figure 1e). Non-insulin treated D rats were underweight as compared to all groups.

3.2 Insulin and metabolite levels at sacrifice (HbA1c, Insulin/c-peptide, BAA, Ketone)

At the time of sacrifice HbA1c, rat c-peptide, human insulin, branched-chain amino acids (BAA), and ketones were measured. Whole blood samples were used to measure HbA1c (%) (Figure 2a) which was significantly higher in D animals compared to ND controls. Additionally, HbA1c levels in D/LI animals were also significantly higher when compared to ND controls but much lower than in uncontrolled D animals. HbA1c percentages in the D/EI animals were comparable to levels measured in the ND animals.

To confirm both the induction of diabetes and insulin therapy, serum levels of rat c-peptide (pmol/L) and exogenous human insulin (mU/L) were measured (Figure 2b). Serum levels of rat c-peptide were greatly reduced in all D animal groups (D, D/EI, D/LI). Serum human insulin was undetectable in ND control animals and D animals, while the human insulin was present in the serum of D/EI and D/LI animals demonstrating diffusion of the exogenous human insulin into the circulation.

Serum levels of BAA and ketones (Figure 2c) at sacrifice were both significantly elevated in D animals compared to all other groups. In D/EI and D/LI animal groups, serum levels were comparable to ND control animals. Additionally, no significant differences in serum levels of BAA and ketones between D/EI animals and D/LI animals were observed.

3.3 Body composition analysis

To characterize the physiological effects of diabetes on our animal model, whole body composition analysis was carried out after metabolite analyses and just prior to sacrifice to

measure lean, fat, and fluid mass in terms of both absolute weight (g) and as a percent of total body weight. Measurements of lean, fat and fluid mass showed significantly lower total tissue weights in D animals compared to ND controls (Figure 3a). Additionally, D/LI animals had less measured lean, fat and fluid mass compared to ND control animals. D/EI animals showed only a significant difference in the amount of fat mass measured when compared to ND animals.

Visualizing the body composition data as percent of total body mass (Figure 3b) shows significantly lower lean mass percentage in D animals compared to ND control animals, but significantly higher fat and fluid mass percentage when compared to ND controls. D/EI animals showed comparable lean tissue mass percentage as ND controls. D/LI animals, however, showed a significant increase in lean mass percentage compared to all groups at the time of sacrifice. Both fat and fluid mass percentages were comparable between D/EI animals and ND control animals. D/LI animals showed significantly lower percent fat mass compared to both ND controls and D/EI animals. The fluid mass percentage was not significantly different between ND controls and D/LI animals.

3.4 Biomarkers

We have previously reported a set of diabetes-associated retinal gene expression biomarkers for use in monitoring interventions seeking to reverse the diabetic phenotype in rat models of diabetes (Freeman et al., 2010). This 24 gene set encompasses genes related to inflammation, vascular function, and neuronal signaling (Table 2). We have previously demonstrated that all of these genes are differentially expressed in the retina after 3 months of uncontrolled diabetes in multiple independent cohorts of animals and that the dysregulation occurs after different periods of hyperglycemia and loss of insulin signaling. In timecourse experiments examining 2 weeks, 1 month, and 3 months of uncontrolled diabetes, we demonstrated that changes in expression occur as early as two weeks (C1inh, C1s, Carhsp1, Chi3L1, End2, Gbp2, Hspb1, Jak3, Kcne2, Lama5, Lgals3, Lgals3bp, Nppa, Pedf, Timp) or at some time after 1 month and before 3 months (Ccr5, Dcamkl1, Ednrb, Icam1, Mct1, Pcgf1, Slc6a11, Stat3, Tnfrsf12a) (Freeman et al., 2010). In agreement with previous findings, all biomarker transcripts were differentially expressed (ANOVA, BH-MTC) with the exceptions of Ednrb, Lama5, Pcgf1, and Pedf which did not reach significance and pass multiple testing correction (Supplemental Table 1, Figure 4a). All of the genes found to be differentially expressed were either upregulated or downregulated in D as compared to ND controls (SNK post-hoc) and in agreement with our previous findings. The sole exception was Slc611 which was only significantly different in the D/EI vs D sample comparison. In both D/EI and D/LI groups, dysregulation of gene expression with diabetes was significantly normalized towards ND levels by insulin treatment (ie., D/EI and D/LI were statistically different from D), and no differences were observed between D/EI, D/LI and ND groups, with the exception of Stat3 expression remaining higher in the D/LI vs ND sample comparison.

Gene expression for all of the genes examined with the exception of Lama5 and Pedf significantly correlated (Pearson’s correlation, BH-MTC) to BG levels and with the exception of Pedf also correlated to HbA1c percentage. As these genes are dysregulated

with diabetes this could be expected and a more informative correlation could be to BG, HbA1c, and ketones in the ND, D/EI, and D/LI groups alone. Examining only those three groups, Edn2, Ednrb, and Timp1 gene expression were positively correlated (Person's correlation, BH-MTC) to BG and HbA1c (%) at sacrifice. Gene expression of Hspb1, Edn2 and Lgals3 were found to have significant positive correlations to ketone levels at sacrifice (Person's correlation, BH-MTC).

When samples were subjected to hierarchical clustering (Figure 4a), the D animals clustered apart from all of the ND, D/EI, and D/LI animals. K-means clustering into 4 groups segregated the D animals into 2 clusters and the ND, D/EI, and D/LI animals into another 2 clusters (not shown). To further compare the pattern of expression in the D/EI and D/LI groups, a support vector machine classifier was built with the data from the ND and D groups. D/EI and D/LI were then assessed using the classifier to determine whether they were classified as more similar to ND or D. In all cases, the D/EI and D/LI animals were classified as ND (Figure 4b). The relationship between samples was also visualized by principal component analysis. The D group animals segregated from the ND, D/EI and D/LI groups which formed a broad constellation (Figure 4c). Some spread in the ND, D/EI, D/LI sample cluster is evident, likely reflecting inter-animal variance.

3.5 Glial IHC and qPCR

GFAP IHC staining of flat-mount retinas was used to assess astrocyte morphology. In ND controls, astrocytes exhibited a stellate morphology with numerous thin, highly ramified processes and spatial compartmentalization (Figure 5a). Intensity of GFAP immunoreactivity was qualitatively increased in astrocytes of D animals, which displayed hypertrophic processes and increased cellular overlap indicative of astrocyte activation. In both D/EI and D/LI groups staining intensity and cell morphology was qualitatively equivalent to ND controls.

Microglial activation was visualized by Iba1 immunoreactivity in vertical cryosections. A low degree of immunoreactivity was evident in ND controls, in well-defined processes in the inner plexiform layer (IPL) and more diffuse staining in the outer plexiform layer (OPL) and photoreceptor outer segments (Figure 5b). Iba1 immunoreactivity was markedly increased in D animals, particularly in cell bodies in the ganglion cell layer (GCL) and processes in the IPL. Both the D/EI and D/LI groups exhibited immunoreactivity qualitatively equivalent to ND controls.

In conjunction with the GFAP IHC, GFAP mRNA expression was assessed. GFAP expression was markedly increased in D animals but was equivalent among animals from ND, D/EI, and D/LI groups (Figure 5c). To further assess inflammatory status, gene expression of the MHC class II invariant chain, CD74, and alpha and beta subunits (RT1-DRA, RT1-DRB, RT1-DMB) were examined in all groups. For all four MHCII genes examined, increased expression was observed in D compared to both ND and insulin treated D groups (D/EI and D/LI).

3.6 Synapse IHC

Qualitative visualization and relative quantification of synaptophysin immunoreactive puncta (SYP-IR) number were performed on retinal sections. Synaptophysin is a pre-synaptic marker shown to be useful as a surrogate measure of synapse number (Masliah et al., 1989; Stroemer et al., 1992). Retinal sections were also counterstained with Hoechst to allow identification of the nuclear cell layers of the retina of representative images (Figure 6a). When compared to ND controls, decreased total SYP-IR was evident in the IPL and OPL of D animals. D/EI and D/LI groups exhibited less total SYP-IR puncta compared to ND controls in the IPL. However, D/EI retained the majority of the total SYP-IR puncta number in the OPL when compared to D and D/LI images. Higher magnification images of the synaptic layers in Figure 6a demonstrate the losses in total SYP-IR as described above (Figure 6b). Counts of SYP-IR puncta within the retinal synapse layers were normalized to ND controls to determine relative quantity of SYP-IR puncta number (Figure 6c). In the OPL, D/EI animals retained SYP-IR puncta numbers when compared to ND controls, and had significantly higher levels of SYP-IR puncta when compared to D and D/LI groups. SYP-IR puncta in the IPL were significantly decreased in all D groups (D, D/EI, D/LI) with IPL SYP-IR puncta numbers trending higher in the D/EI animals.

4. Discussion

This study used Sprague Dawley rats, including ND and STZ-induced D animals; with two insulin intervention groups including D/EI and D/LI to investigate the effects of diabetes and insulin therapy on biomarkers of DR as well as inflammation and neuronal deficits associated with DR. Insulin intervention, despite the length of uncontrolled diabetes, was able to prevent or reverse changes in BG, HbA1c, BAA, ketones, body mass, gene expression biomarkers and inflammatory markers associated with diabetes. The surrogate marker of retinal synapse numbers, SYP-IR, was decreased in animals. Early intervention with insulin prevented some of the synapse loss while late insulin intervention was unable to restore loss of synapses in the retina. This is the first demonstration that markers of synapse loss, once extant, are not reversed with insulin treatment, displaying a metabolic memory phenotype at the cellular level.

The body composition data show decreased total weight of D animals compared to the D/EI, D/LI and ND controls. Additionally, the absolute measurements of lean, fat, and fluid tissue were comparable between ND controls and D/EI animals, with D/LI animals trending towards ND and regaining mass. The Diabetes Control and Complications Trial showed weight gain in the form of both total lean and total fat mass with intensive insulin therapy patients (DCCT Group, 2001). Acute insulin therapy has been shown to increase lean mass, then subsequently increase fat and lean mass (Wang et al., 2013). This phenomenon is apparent in our animals as well, where we see a significant increase in the lean mass percentage of D/LI animals compared to both ND controls and D/EI animals. We also observed a complete normalization of fat mass percent equivalent to ND controls in the D/EI animals, while the D/LI animals' fat mass percentage is significantly lower. These results are concordant with previous studies showing lean mass increasing within 6 months of insulin therapy in humans, and fat mass increasing between 6–12 months after onset of

insulin therapy (Rosenfalck et al., 2002). Our results show similar trends in the percent mass where the fat mass percentage of D/LI animals has yet to normalize due to the shorter duration of insulin therapy. The relatively new ability to readily analyze body composition in rodent models provides a new window on systemic metabolic status of animals in preclinical studies.

Longitudinal assessment of *in vivo* retinal gene expression is not possible within one animal, but analysis of the mRNA expression of previously described diabetic retina biomarker genes from this animal model (Freeman et al., 2010) provides additional context for the effects of differing histories of insulin therapy on retinal phenotype. These gene expression changes have been demonstrated to occur quickly, as early as 2 weeks of uncontrolled diabetes (C1inh, C1s, Carhsp1, Chi3L1, End2, Gbp2, Hspb1, Jak3, Kcne2, Lama5, Lgals3, Lgals3bp, Nppa, Pedf, Timp) or after a longer duration of uncontrolled diabetes [greater than 1 month and less than 3 months (Ccr5, Dcamkl1, Ednrb, Icam1, Mct1, Pcgf1, Slc6a11, Stat3, Tnfrsf12a)]. The RNA expression levels of these biomarker genes were not statistically different in the ND versus D/EI or between ND versus D/LI comparisons, with the exception of Stat3. For gene expression changes occurring by 2 weeks of diabetes the late intervention group normalizes these changes, which should already be extant by the time of insulin intervention. These results also agree with our previous findings that for many diabetes-associated retinal gene expression changes, the expression levels are normalized after a period insulin treatment (Bixler et al., 2011). For those changes that only occur later, >1 month, the early insulin intervention presumably prevents these changes from occurring. The normalization of all of these biomarkers to a pattern similar to that seen in ND animals demonstrates that these genes do not fit the metabolic memory phenotype (Bixler et al., 2011; Pirola et al., 2010; Villeneuve et al., 2011). Separate transcriptomic studies are currently in progress seeking to identify genes which fit the metabolic memory phenotype and their potential regulatory mechanisms, such as epigenetic changes. Furthermore, the finding that the expression of these genes is normalized with insulin treatment suggests that insulin treatment groups should be included in preclinical studies to provide a more clinically relevant picture of retinal gene expression.

Inflammation is a likely causative process in diabetic complications, including DR. Retinal inflammation associated with diabetes was investigated through astrocytic and microglial activation and gene expression markers of inflammation. Previously, induction of GFAP, a glial cell marker of induced inflammation, has been reported to increase with uncontrolled diabetes after 1–3 months of diabetes with that induction potentially subsiding with longer durations of diabetes (Barber et al., 2000; Lieth et al., 1998). The data presented here corroborate previous studies by showing increased qualitative levels of GFAP immunoreactivity and altered astrocyte morphology consistent with astrocyte expression in whole retina flat mounts with uncontrolled diabetes. Here, GFAP immunoreactivity was qualitatively higher after 3 months in D animals when compared to ND controls in agreement with previous findings (Lieth et al., 1998). Additionally, both insulin treated groups show equivalent GFAP immunoreactivity to ND control levels. The qualitative immunoreactivity comparison is bolstered by gene expression data demonstrating the same pattern. When combined with previous data showing an induction of GFAP by 3 months,

but only a small increase by 1 month (Lieth et al., 1998), it is possible to conclude that the early insulin intervention prevented astrocyte activation, while the late intervention reversed activation to control levels. Detailed cell type analysis of the Müller cell populations was not addressed here. Both astrocytes and Müller cells express GFAP in the retina and increased Müller cell expression astrocyte expression with uncontrolled diabetes has been observed (Asnaghi et al., 2003; Barber et al., 2000; Hollander et al., 1991; Lieth et al., 1998; Ly et al., 2011). Here, by using whole retina flat mounts, the increase in GFAP immunoreactivity can most likely be attributed to astrocytes in the inner limiting membrane with some signal from Müller cells oriented end-on (Barber et al., 2000; Li et al., 2002). To more precisely localize GFAP expression of Müller cells and astrocyes, future co-immunolabeling studies will need to be carried out (Gerhardinger et al., 2005).

Retinal microglial activation is known to occur with 4–8 weeks of diabetes (Barber et al., 2005; Ibrahim et al., 2011; Kezic et al., 2013) with cellular morphology changes occurring shortly after diabetes induction (Rungger-Brandle et al., 2000). Similarly, microglial activation and macrophage infiltration into the retina of diabetic rats has been observed at 9 weeks of uncontrolled diabetes (Tsai et al., 2009). Human patients with diabetes also present microglial activation within the retina (Zeng et al., 2008). Gene expression markers of microglial activation, Cd74, and MHCII subunits also showed increased expression in D animals, indicative of increased microglial activation and inflammation with diabetes, when compared to ND control animals. D/EI and E/LI groups demonstrated equivalent levels of both qualitative immunoreactivity and gene expression to that seen in ND controls. The earliest time reported in the literature to microglial activation in experimental DR is 4 weeks in STZ rats (Rungger-Brandle et al., 2000). Therefore, it seems likely that early insulin intervention at 1 week of diabetes prevented microglial activation. Additionally, since late insulin intervention showed the same amount of qualitative immunoreactivity and gene expression as seen in D/EI and ND animals, it can be concluded that D/LI normalized microglial activity. This was the case, more broadly as well, with the gene expression biomarkers and metabolic measures. Therefore, the inflammatory processes examined can be normalized or prevented with insulin intervention, and displays no apparent metabolic memory phenotype. Longer durations of insulin treated diabetes should be informative of whether with extended insulin treatment inflammatory processes begin to increase. Additionally, other aspects of inflammation could remain induced despite insulin intervention, however, these were not addressed here (Yang et al., 2009; Zorena et al., 2013).

Data presented here support previous studies showing early loss of retinal SYP-IR puncta as a surrogate measure of retinal synapse number. Previously we have demonstrated that SYP-IR puncta decrease in the IPL and OPL after 1 and 3 months or uncontrolled diabetes, indicative of synapse loss (VanGuilder et al., 2008). Here the effects of differing durations of uncontrolled diabetes before insulin replacement were investigated. We found loss of SYP-IR puncta to be greater with a longer period of uncontrolled diabetes before insulin treatment when compared to those animals with a significantly shorter period of uncontrolled diabetes before insulin treatment. Synaptophysin is a marker of presynaptic terminals and the fullest prevention of SYP-IR puncta loss occurred with the early insulin treatment in the OPL. Several studies have documented the effects of diabetes on the

ultrastucture of the retina. It has been shown that the retina in the parafoveal area is thinner in DR patients when compared to diabetic patients without retinopathy (Araszkiewicz et al., 2012). Additionally, this study showed the loss of intraretinal neural tissue and neurodegeneration in diabetic patients with retinopathy. The loss in retinal neural tissue and neurodegeneration could be explained initially by loss of synapses. Multiple deficits in neuronal maintenance with diabetes have been demonstrated in retinopathy; mainly, loss of GCL thickness and RGC neurodegeneration (van Dijk et al., 2011; Yang et al., 2012). Together with our previous results, the data presented here suggest that once synapses are lost they are not regained with insulin therapy (D/LI). Furthermore, early insulin (D/EI) therapy does not completely prevent loss of synaptic markers. Longer term studies are needed to examine whether synapse loss continues to progress or if with sufficient time synapses are restored. Additionally, the possibility remains that there is synapse loss in the very first few days of diabetes. Future studies will have to investigate the acute timecourse of initial hours and days of diabetes.

It should also be noted that detailed stereological electron microscopy studies are needed in the future to directly quantify synapse number. While it is unlikely that decreased SYP protein expression could lead to SYP-IR puncta declining below detection, a direct assessment of synapse number instead of through surrogate markers such as these is warranted in the future. Our results extend previous findings by showing loss of synaptic markers in the IPL that is persistent with insulin replacement after an extended period of uncontrolled diabetes and, as such, may represent a cellular form of metabolic memory. These results suggest a deficit in the GCL and IPL compared to the other layers of the retina. Inner retinal activity has also been shown to decrease with diabetes, which could reflect the sensitivity of the IPL to synapse loss (Kohzaki et al., 2008). Because synaptophysin is a pre-synaptic marker, further investigations are needed to address whether there, as could be expected, is a corresponding loss in post-synaptic terminals, and whether there are fewer synapses per neuron or decreased numbers of neurons due to apoptosis. Additionally, more investigation needs to be dedicated to determine why the IPL is more sensitive to synapse loss compared to the OPL.

These findings emphasize the need to include insulin intervention groups in preclinical diabetes studies, and demonstrate that while immediate insulin replacement therapy may prevent the development of many phenomena, changes that develop before initiation of insulin therapy may or may not be readily normalized by standard insulin treatment. Not only does including insulin treatment groups in preclinical studies more faithfully represent the clinical population, but the findings presented here suggest that insulin prevents or normalizes a significant amount of systemic metabolic and retinal molecular changes with diabetes. Including insulin intervention groups will be important for preclinical studies seeking to develop therapies for treating DR. Previous reports have used uncontrolled diabetic rodent models and evaluated the effects of anti-inflammatory agents on inflammation associated with DR without an insulin treatment group (Tsai et al., 2009; Yang et al., 2009). Including an insulin treatment group in interventional studies would clarify the actions of investigational agents as an adjunct to standard metabolic control via insulin.

5. Conclusions

Growth, body composition, and metabolic measures of diabetes were all normalized with insulin treatment regardless of the duration of uncontrolled diabetes prior to initiation of insulin therapy. Previous studies have demonstrated retinal neuroinflammation is markedly induced with diabetes; however this can be placated with insulin treatment after either short or extended periods of uncontrolled diabetes. Additionally, our results indicate that once markers of retinal synapse loss occur during uncontrolled diabetes, subsequent restoration of normoglycemia and insulin signaling may not be sufficient to restore neuronal synaptic populations to their normal levels.

Supplementary Material

Refer to Web version on PubMed Central for supplementary material.

Acknowledgments

The authors wish to thank Carson Wells for assistance with figure preparation, Penn State College of Medicine Genome Sciences Facility for assistance with gene expression measurements, and Dr. Christopher Lynch for use of body composition instrumentation and assistance with the BAA assay. This work was supported by NIH/NEI (R01EY021716), Pennsylvania Tobacco Settlement Funds, and Penn State Hershey Eye Center grants.

References

Aiello LP. DCCT/EDIC Research Group. Diabetic retinopathy and other ocular findings in the diabetes control and complications trial/epidemiology of diabetes interventions and complications study. Diabetes Care. 2014; 37:17–23. [PubMed: 24356593]

Antonetti DA, Barber AJ, Bronson SK, Freeman WM, Gardner TW, Jefferson LS, Kester M, Kimball SR, Krady JK, LaNoue KF, Norbury CC, Quinn PG, Sandirasegarane L, Simpson IA, Group JDRC. Diabetic retinopathy: seeing beyond glucose-induced microvascular disease. Diabetes. 2006; 55:2401–2411. [PubMed: 16936187]

Antonetti DA, Klein R, Gardner TW. Diabetic retinopathy. New England J Med. 2012; 366:1227–1239. [PubMed: 22455417]

Araszkiewicz A, Zozulinska-Ziolkiewicz D, Meller M, Bernardczyk-Meller J, Pilacinski S, Rogowicz-Frontczak A, Naskret D, Wierusz-Wysocka B. Neurodegeneration of the retina in type 1 diabetic patients. Polskie Archiwum Medycyny Wewnetrznej. 2012; 122:464–470. [PubMed: 22910230]

Asnaghi V, Gerhardinger C, Hoehn T, Adeboje A, Lorenzi M. A role for the polyol pathway in the early neuroretinal apoptosis and glial changes induced by diabetes in the rat. Diabetes. 2003; 52:506–511. [PubMed: 12540628]

Aung MH, Kim MK, Olson DE, Thule PM, Pardue MT. Early visual deficits in streptozotocin-induced diabetic long evans rats. Invest Ophthalmol Vis Sci. 2013; 54:1370–1377. [PubMed: 23372054]

Barber AJ, Antonetti DA, Gardner TW. The Penn State Retina Research Group. Altered expression of retinal occludin and glial fibrillary acidic protein in experimental diabetes. Invest Ophthalmol Vis Sci. 2000; 41:3561–3568. [PubMed: 11006253]

Barber AJ, Antonetti DA, Kern TS, Reiter CE, Soans RS, Krady JK, Levison SW, Gardner TW, Bronson SK. The Ins2Akita mouse as a model of early retinal complications in diabetes. Investigative ophthalmology & visual science. 2005; 46:2210–2218. [PubMed: 15914643]

Barber AJ, Gardner TW, Abcouwer SF. The significance of vascular and neural apoptosis to the pathology of diabetic retinopathy. Invest Ophthalmol Vis Sci. 2011; 52:1156–1163. [PubMed: 21357409]

Barber AJ, Lieth E, Khin SA, Antonetti DA, Buchanan AG, Gardner TW. Neural apoptosis in the retina during experimental and human diabetes. Early onset and effect of insulin. J Clin Invest. 1998; 102:783–791. [PubMed: 9710447]

Beckett PR. Spectrophotometric assay for measuring branched-chain amino acids. Methods in Enzymology. 2000; 324:40–47. [PubMed: 10989416]

Benjamini Y, Drai D, Elmer G, Kafkafi N, Golani I. Controlling the false discovery rate in behavior genetics research. Behavioural Brain Res. 2001; 125:279–284.

Bixler GV, Vanguilder HD, Brucklacher RM, Kimball SR, Bronson SK, Freeman WM. Chronic insulin treatment of diabetes does not fully normalize alterations in the retinal transcriptome. BMC Medical Genomics. 2011; 4:40. [PubMed: 21575160]

Brucklacher RM, Patel KM, VanGuilder HD, Bixler GV, Barber AJ, Antonetti DA, Lin CM, LaNoue KF, Gardner TW, Bronson SK, Freeman WM. Whole genome assessment of the retinal response to diabetes reveals a progressive neurovascular inflammatory response. BMC Medical Genomics. 2008; 1:26. [PubMed: 18554398]

Engerman RL, Kern TS. Progression of incipient diabetic retinopathy during good glycemic control. Diabetes. 1987; 36:808–812. [PubMed: 3556280]

Fernandez DC, Pasquini LA, Dorfman D, Aldana Marcos HJ, Rosenstein RE. Early distal axonopathy of the visual pathway in experimental diabetes. Am J Path. 2012; 180:303–313. [PubMed: 22079928]

Freeman WM, Bixler GV, Brucklacher RM, Lin CM, Patel KM, VanGuilder HD, LaNoue KF, Kimball SR, Barber AJ, Antonetti DA, Gardner TW, Bronson SK. A multistep validation process of biomarkers for preclinical drug development. The Pharmacogenomics J. 2010; 10:385–395.

Gastinger MJ, Singh RS, Barber AJ. Loss of cholinergic and dopaminergic amacrine cells in streptozotocin-diabetic rat and Ins2Akita-diabetic mouse retinas. Invest Ophthalmol Vis Sci. 2006; 47:3143–3150. [PubMed: 16799061]

Gaucher D, Chiappore JA, Paques M, Simonutti M, Boitard C, Sahel JA, Massin P, Picaud S. Microglial changes occur without neural cell death in diabetic retinopathy. Vision research. 2007; 47:612–623. [PubMed: 17267004]

Gerhardinger C, Costa MB, Coulombe MC, Toth I, Hoehn T, Grosu P. Expression of acute-phase response proteins in retinal Muller cells in diabetes. Invest Ophthalmol Vis Sci. 2005; 46:349–357. [PubMed: 15623795]

Group T.D.C.a.C.T.R. Influence of intensive diabetes treatment on body weight and composition of adults with type 1 diabetes in the Diabetes Control and Complications Trial. Diabetes Care. 2001; 24:1711–1721. [PubMed: 11574431]

Hollander H, Makarov F, Dreher Z, van Driel D, Chan-Ling TL, Stone J. Structure of the macroglia of the retina: sharing and division of labour between astrocytes and Muller cells. J Comp Neuro. 1991; 313:587–603.

Ibrahim AS, El-Remessy AB, Matragoon S, Zhang W, Patel Y, Khan S, Al-Gayyar MM, El-Shishtawy MM, Liou GI. Retinal microglial activation and inflammation induced by amadori-glycated albumin in a rat model of diabetes. Diabetes. 2011; 60:1122–1133. [PubMed: 21317295]

Intine RV, Sarras MP Jr. Metabolic memory and chronic diabetes complications: potential role for epigenetic mechanisms. Current Diabetes Reports. 2012; 12:551–559. [PubMed: 22760445]

Jackson GR, Barber AJ. Visual dysfunction associated with diabetic retinopathy. Current Diabetes Reports. 2010; 10:380–384. [PubMed: 20632133]

Kastelan S, Tomic M, Gverovic Antunica A, Salopek Rabatic J, Ljubic S. Inflammation and pharmacological treatment in diabetic retinopathy. Mediators Inflamm. 2013; 2013:213130. [PubMed: 24288441]

Kern TS, Barber AJ. Retinal ganglion cells in diabetes. J Phys. 2008; 586:4401–4408.

Kezic JM, Chen X, Rakoczy EP, McMenamin PG. The effects of age and Cx3cr1 deficiency on retinal microglia in the Ins2(Akita) diabetic mouse. Invest Ophthalmol Vis Sci. 2013; 54:854–863. [PubMed: 23307960]

Kohzaki K, Vingrys AJ, Bui BV. Early inner retinal dysfunction in streptozotocin-induced diabetic rats. Invest Ophthalmol Vis Sci. 2008; 49:3595–3604. [PubMed: 18421077]

Lai AK, Lo AC. Animal models of diabetic retinopathy: summary and comparison. J Diabetes Res. 2013; 2013:106594. [PubMed: 24286086]

Li Q, Zemel E, Miller B, Perlman I. Early retinal damage in experimental diabetes: electroretinographical and morphological observations. Exp Eye Res. 2002; 74:615–625. [PubMed: 12076083]

Lieth E, Barber AJ, Xu B, Dice C, Ratz MJ, Tanase D, Strother JM. Penn State Retina Research Group. Glial reactivity and impaired glutamate metabolism in short-term experimental diabetic retinopathy. Diabetes. 1998; 47:815–820. [PubMed: 9588455]

Ly A, Yee P, Vessey KA, Phipps JA, Jobling AI, Fletcher EL. Early inner retinal astrocyte dysfunction during diabetes and development of hypoxia, retinal stress, and neuronal functional loss. Invest Ophthalmol Vis Sci. 2011; 52:9316–9326. [PubMed: 22110070]

Masliah E, Terry RD, DeTeresa RM, Hansen LA. Immunohistochemical quantification of the synapse-related protein synaptophysin in Alzheimer disease. Neurosci Letters. 1989; 103:234–239.

Pietropaolo M, Barinas-Mitchell E, Kuller LH. The heterogeneity of diabetes: unraveling a dispute: is systemic inflammation related to islet autoimmunity? Diabetes. 2007; 56:1189–1197. [PubMed: 17322478]

Pirola L, Balcerczyk A, Okabe J, El-Osta A. Epigenetic phenomena linked to diabetic complications. Nature reviews Endocrinology. 2010; 6:665–675.

Rosenfalck AM, Almdal T, Hilsted J, Madsbad S. Body composition in adults with Type 1 diabetes at onset and during the first year of insulin therapy. Diabetic Med. 2002; 19:417–423. [PubMed: 12027931]

Rungger-Brandle E, Dosso AA, Leuenberger PM. Glial reactivity, an early feature of diabetic retinopathy. Invest Ophthalmol Vis Sci. 2000; 41:1971–1980. [PubMed: 10845624]

Stroemer RP, Kent TA, Hulsebosch CE. Increase in synaptophysin immunoreactivity following cortical infarction. Neurosci Letters. 1992; 147:21–24.

Tang J, Kern TS. Inflammation in diabetic retinopathy. Prog Retin Eye Res. 2011; 30:343–358. [PubMed: 21635964]

Tsai GY, Cui JZ, Syed H, Xia Z, Ozerdem U, McNeill JH, Matsubara JA. Effect of N-acetylcysteine on the early expression of inflammatory markers in the retina and plasma of diabetic rats. Clin & Exper Ophth. 2009; 37:223–231.

van Dijk HW, Verbraak FD, Stehouwer M, Kok PH, Garvin MK, Sonka M, DeVries JH, Schlingemann RO, Abramoff MD. Association of visual function and ganglion cell layer thickness in patients with diabetes mellitus type 1 and no or minimal diabetic retinopathy. Vision Res. 2011; 51:224–228. [PubMed: 20801146]

VanGuilder HD, Bixler GV, Kutzler L, Brucklacher RM, Bronson SK, Kimball SR, Freeman WM. Multi-modal proteomic analysis of retinal protein expression alterations in a rat model of diabetic retinopathy. PloS One. 2011; 6:e16271. [PubMed: 21249158]

VanGuilder HD, Brucklacher RM, Patel K, Ellis RW, Freeman WM, Barber AJ. Diabetes downregulates presynaptic proteins and reduces basal synapsin I phosphorylation in rat retina. Euro J Neurosci. 2008; 28:1–11.

Villeneuve LM, Reddy MA, Natarajan R. Epigenetics: deciphering its role in diabetes and its chronic complications. Clin Exper Pharm Phys. 2011; 38:451–459.

Wang H, Ni YF, Li HZ, Yang S, Feng B. Effects of insulin monotherapy on body weight, composition, and fat distribution in newly diagnosed patients with Type 2 diabetes mellitus. J Diabetes. 2013; 5:146–148. [PubMed: 23316885]

Yang LP, Sun HL, Wu LM, Guo XJ, Dou HL, Tso MO, Zhao L, Li SM. Baicalein reduces inflammatory process in a rodent model of diabetic retinopathy. Invest Ophthalmol Vis Sci. 2009; 50:2319–2327. [PubMed: 19011009]

Yang Y, Mao D, Chen X, Zhao L, Tian Q, Liu C, Zhou BL. Decrease in retinal neuronal cells in streptozotocin-induced diabetic mice. Mol Vis. 2012; 18:1411–1420. [PubMed: 22690119]

Zeng HY, Green WR, Tso MO. Microglial activation in human diabetic retinopathy. Arch Ophthal. 2008; 126:227–232. [PubMed: 18268214]

Zhang L, Chen B, Tang L. Metabolic memory: mechanisms and implications for diabetic retinopathy. Diabetes research and clinical practice. 2012; 96:286–293. [PubMed: 22209677]

Zorena K, Raczynska D, Raczynska K. Biomarkers in Diabetic Retinopathy and the Therapeutic Implications. Mediators Inflamm. 2013; 2013:193604. [PubMed: 24311895]

Highlights

- Early insulin intervention prevents loss of retinal synaptic markers in experimental diabetes
- Insulin intervention normalizes common neuroinflammatory biomarkers associated with diabetes
- Retinal synapses may represent a cellular form of metabolic memory phenotype with diabetes

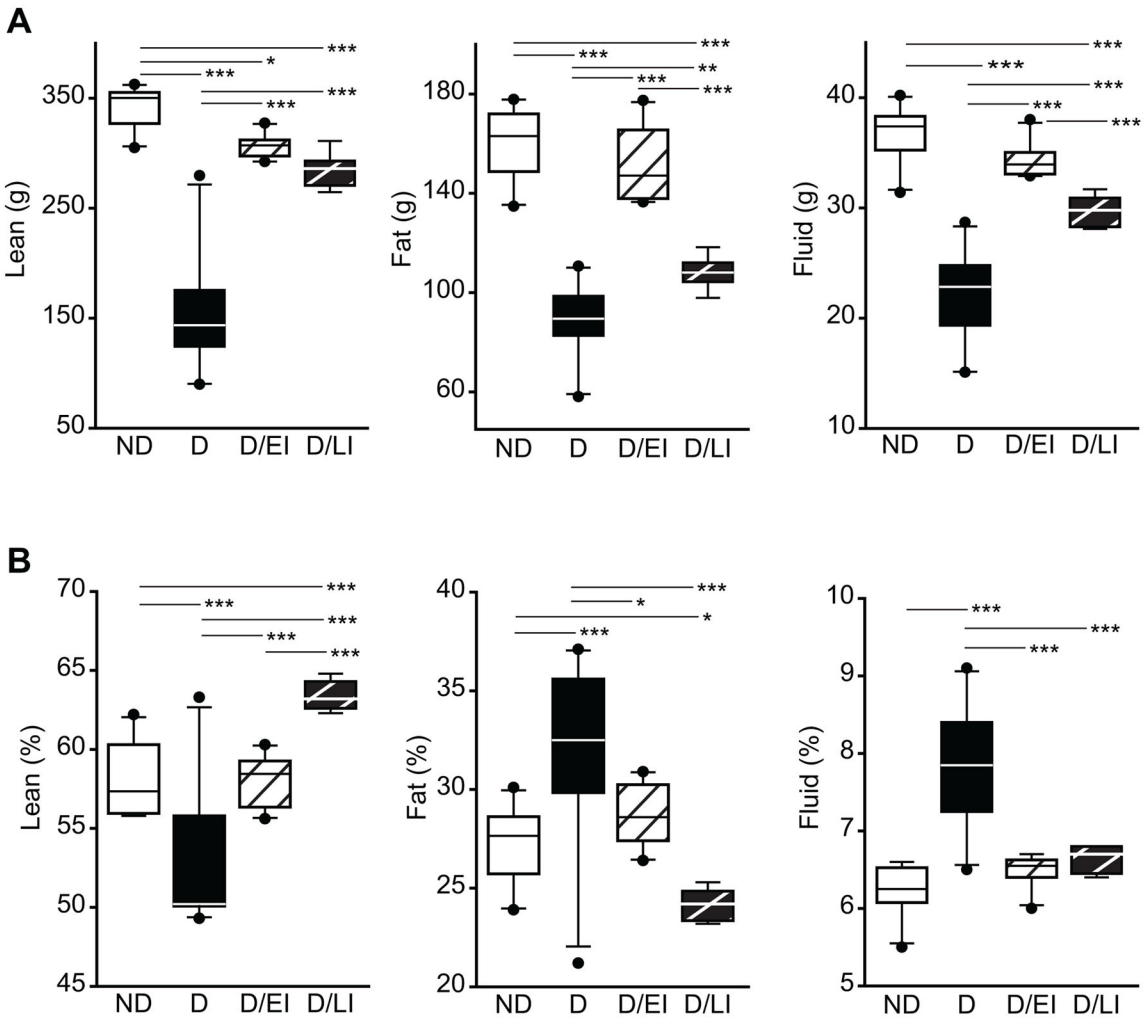

Figure 1. Experimental design and longitudinal tracking of blood glucose and body weight[§]

A) A twelve-week duration of STZ-induced diabetes was investigated, including uncontrolled diabetic (D) and insulin-treated diabetic groups. D animals were placed into three groups that either received no insulin treatment, insulin treatment starting 1 week after diabetes induction (diabetic/early intervention – D/EI), insulin treatment starting 6 weeks after diabetes induction (diabetic/late intervention – D/LI). The non-diabetic group (ND) received citrate injection at the same time as the diabetic animals received STZ. All animals were sacrificed after 3 months. **B)** Blood glucose (BG) was monitored throughout the study. BG was determined every two weeks and during insulin treatment BG was determined weekly to monitor treatment performance. **C)** At sacrifice BG was higher in D animals than in all other groups, while BG in D/LI animals was higher than in the ND and D/EI groups. **D)** Body weights were monitored throughout the study. In D groups weight gain was slower than in ND animals but normal growth rates were regained upon insulin treatment. **E)** At sacrifice all D groups weighed less than ND controls and insulin treated diabetic groups (D/EI and D/LI) were heavier than untreated D animals depending on the length of treatment. ANOVA, SNK post hoc ***pitalic>0.001, ** pbold>0.01, *p<0.05. [§] Data presented are derived from rats in two experimental cohorts (n=20/group).

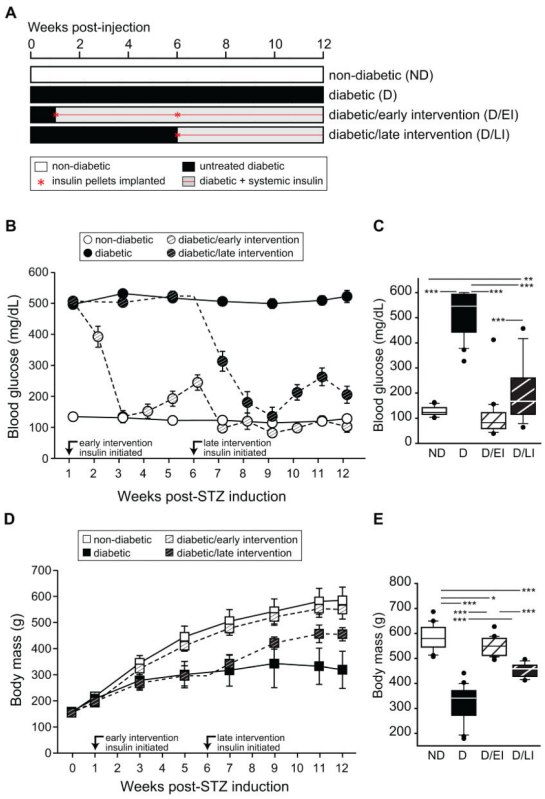

Figure 2. Insulin and metabolic measurements at sacrifice

A) Glycosylated hemoglobin (HbA1c) levels were elevated in uncontrolled diabetic animals (D) as compared to all other groups, with the diabetic/late intervention (D/LI) group demonstrating higher levels as compared to the ND and diabetic/early intervention (D/EI) groups. **B)** To assess endogenous and exogenous insulin levels, rat c-peptide and human insulin levels were determined at sacrifice. D groups demonstrated very low levels of c-peptide as compared to ND animals. Equivalent levels of human insulin were evident in both the D/EI and D/LI groups and no human insulin was detected in the non-insulin treated groups. **C)** Branched-chain amino acid (BAA) and ketone levels were elevated at sacrifice as compared to ND and insulin treated diabetic groups (D/EI and D/LI). ANOVA, SNK post hoc ***p<0.001. Cohort 2 (n=10/group), § - Not detected.

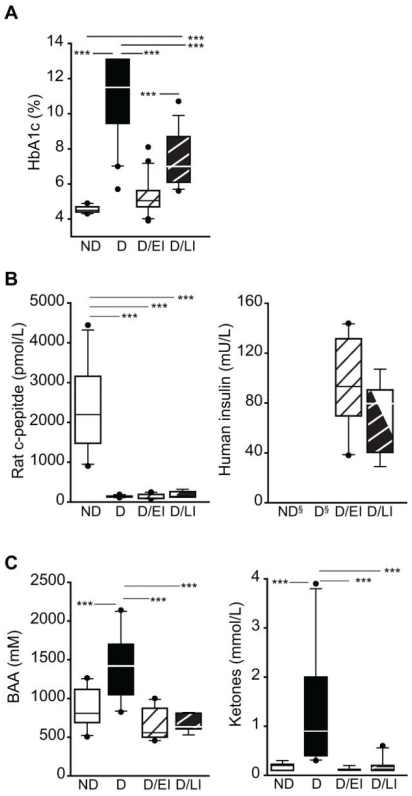

Figure 3. Body composition analysis

At sacrifice fat, lean, and fluid mass were determined by whole body NMR and expressed as both weight (g) **(A)** and as percentage of body weight **(B)**. Early intervention with insulin (D/EI) prevented diabetes induced changes observed in diabetic (D) animals, while later insulin intervention (D/LI) partially normalized body composition to non-diabetic (ND) control levels. ANOVA, SNK post hoc ***p<0.001, ** p<0.01, *p<0.05. Cohort 2 (n=10/group).

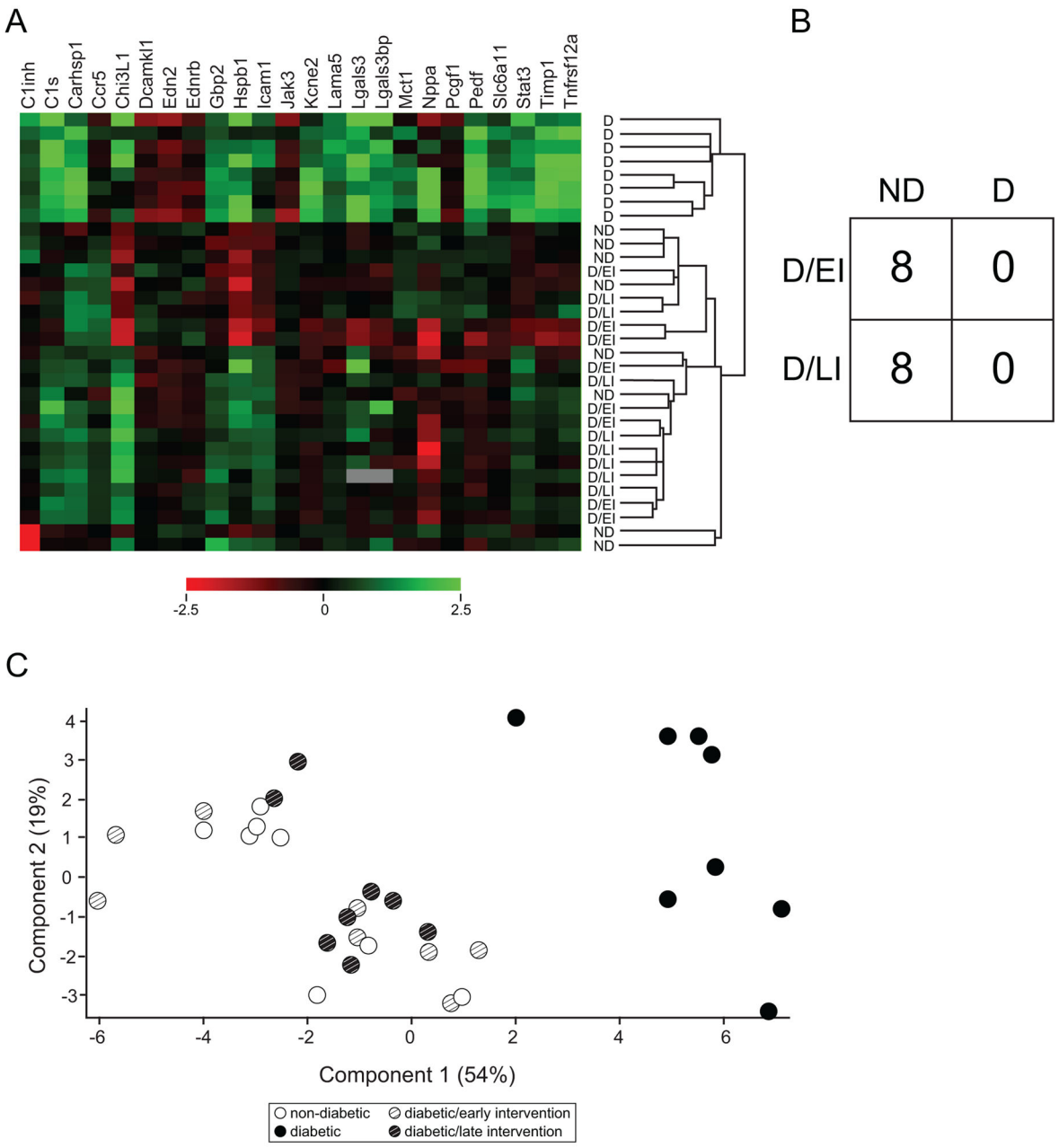

Figure 4. Diabetes-associated retinal gene expression biomarker response to insulin intervention

Previously we have described diabetes associated retinal gene expression biomarkers and here examined their expression in all groups. As with previous studies, uncontrolled diabetic (D) animals demonstrated significant dysregulation of gene expression compared to non-diabetic (ND) controls. Insulin treated groups, diabetic/early intervention (D/EI) and diabetic/late intervention (D/LI), showed gene expression normalized to ND control levels. As presented in a heatmap **(A)**, D animals separated together and away from ND animals. ND and insulin treated D animals (D/EI and D/LI animals) were intermixed. **B)** To assess more empirically if insulin treated D animals had a gene expression profile more like ND or D a support vector machine algorithm was used to generate a classification pattern for ND

and D. When D/EI and D/LI animals were subsequently tested against the pattern all insulin treated diabetic animals were classified as having a ND pattern. **C)** When visualized by a principal components plot using the biomarker data, the D animals (each spot represents an individual animal) separated from the animals in the other groups, Cohort 1 (n=8/group).

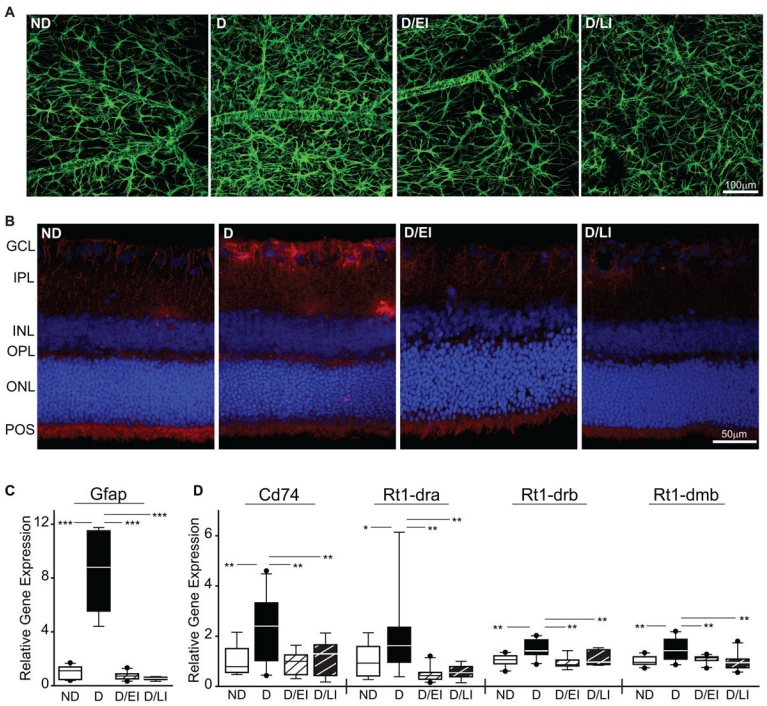

Figure 5. Retinal inflammation

(A) Astrocyte activation was assessed through GFAP staining in whole retina flat-mounts. Elevated GFAP immunoreactivity and altered cellular morphology were evident in uncontrolled diabetic (D) animals as compared to non-diabetic (ND) controls and insulin treated diabetic/early intervention (D/EI) and diabetic/late intervention (D/LI). Cohort 2 (n=5). **(B)** Microglial activation was visualized by immunoreactivity to Iba1 in vertical cryosections. Elevated Iba1 staining was observed in the GCL and IPL of D animals compared to all other groups. Cohort 2 (n=5). **(C)** Whole retina GFAP mRNA levels were increased in D animals, but normalized to ND control levels in D/EI and D/LI groups. **(D)** MHCII family mRNAs in whole retina preparations were induced in D animals as compared to all other groups. ANOVA, SNK post hoc ***p<0.001, ** p<0.01, *p<0.05. cohort 1 (n=10/group),; GCL – ganglion cell layer, IPL – inner plexiform layer, INL – inner nuclear layer, OPL – outer plexiform layer, ONL – outer nuclear layer, POS – photoreceptor outer segments.

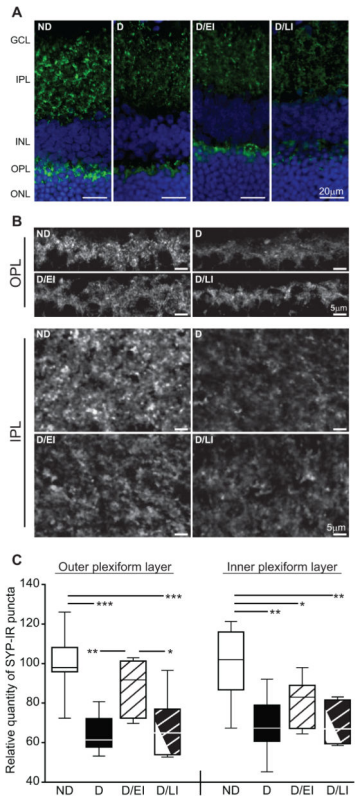

Figure 6. Retinal synapse quantitation

A) Retinal synaptophysin immunoreactivity (SYP-IR), assessed as a marker of synaptic terminals, was distributed throughout IPL and OPL as punctate staining. There was qualitatively less immunoreactivity in both plexiform layers of uncontrolled diabetic (D) rats compared to non-diabetic (ND) controls. This decreased in qualitative immunoreactivity was attenuated by insulin replacement in the diabetic/early intervention (D/EI) group, while the appearance of the diabetic/late intervention (D/LI) group was closer to that of the D animals. **B)** High-magnification images of retinal plexiform layers demonstrate a decrease in the intensity of SYP-IR as well as an apparent reduction in the number of SYP-IR puncta in the IPL and OPL of D rats, with similar profiles observed in D/LI group. SYP-IR in the OPL of the D/EIgroup was qualitatively similar to that of ND controls, although reduced staining was apparent in the IPL. **C)** Automated quantitation of SYP-IR puncta numbers revealed significant decreases after twelve weeks of uncontrolled diabetes compared to age-matched ND controls. Insulin treatment in the D/EI group prevented synapse loss in the OPL, but not the IPL. SYP-IR puncta numbers in the D/LI group were reduced to a similar extent as that observed in D rats, suggesting that six weeks of insulin replacement following six weeks of uncontrolled diabetes is not sufficient to prevent or reverse loss of SYP-IR puncta. ANOVA/SNK, *$p<0.05$, **$p<0.01$, ***$p<0.001$, cohorts 1 and 2 (n=8/group).GCL – ganglion cell layer, IPL – inner plexiform layer, INL – inner nuclear layer, OPL – outer plexiform layer, ONL – outer nuclear layer.

Table 1

Cohort information*

		n/group	insulin treatment	BG (mg/dL)	Hba1c (%)	Mass (g)	additional endpoints
Cohort 1	Nondiabetic	10	N/A	140 ± 5.4	4.5 ± 0.06	580 ± 18.8	Biomarker panel expression, inflammatory gene expression, synapse quantitation
	Uncontrolled diabetic	10	N/A	568 ± 10.5	12.4 ± 0.40	362 ± 10.0	
	Diabetic/early intervention	10	weeks 1–12	108 ± 9.4	5.1 ± 0.29	570 ± 9.9	
	Diabetic/late intervention	10	weeks 6–12	280 ± 36.7	7.7 ± 0.40	460 ± 7.9	
Cohort 2	Nondiabetic	10	N/A	118 ± 3.0	4.6 ± 0.06	589 ± 13.5	Whole-body NMR, serum c- peptide/human insulin, Gfap/Iba1 imaging, synapse quantitation
	Uncontrolled diabetic	10	N/A	477 ± 29.3	9.7 ± 0.68	279 ± 22.3	
	Diabetic/early intervention	10	weeks 1–12	97 ± 35.8	5.3 ± 0.37	529 ± 9.5	
	Diabetic/late intervention	10	weeks 6–12	122 ± 13.2	7.1 ± 0.59	449 ± 8.5	

*BG: blood glucose, HbA1c: glycated hemoglobin; data collected at sacrifice.

Table 2

Gene expression primer/probe sets.

Gene ID	Assay ID	Gene Name	Alias
C1-Inh	Rn01485600_m1	serine (or cysteine) peptidase inhibitor, clade G, member 1	Serping1
C1s	Rn00594278_m1	complement component 1, s subcomponent	r-gsp
Carhsp1	Rn00596083_m1	calcium regulated heat stable protein 1	Crhsp-24, Crhsp24
Ccr	Rn00588629_m1	chemokine (C-C motif) receptor 5	Ckr5, Cmkbr5
Cd74	Rn00565062_m1	Cd74 molecule, major histocompatibility complex, class II invariant chain	INVG34
Chi3l1	Rn01490608_m1	chitinase 3-like 1	MGC109420
Dcamkl1	Rn00584294_m1	doublecortin-like kinase 1	Dclk1, Cpg16
Edn2	Rn00561135_m1	endothelin 2	Et2
Ednrb	Rn00569139_m1	endothelin receptor type B	Ednra, Etb
Gbp2	Rn00592467_m1	guanylate nucleotide binding protein 2	MGC93208
Gfap	Rn00566603_m1	glial fibrillary acidic protein	
Hspb1	Rn00583001_g1	heat shock protein 1	Hsp25, Hsp27
Icam1	Rn00564227_m1	intercellular adhesion molecule 1	CD54, ICAM
Jak3	Rn00563431_m1	Janus kinase 3	RATJAK3
Kcne2	Rn02094913_s1	potassium voltage-gated channel, Isk-related subfamily, gene 2	MGC108602, Mirp1
Lama5	Rn01415966_g1	laminin alpha 5	
Lgals3	Rn00582910_m1	lectin, galactose binding, soluble 3	MGC105387, gal-3
Lgals3bp	Rn00478303_m1	lectin, galactoside-binding, soluble, 3 binding protein	Ppicap
Mct1	Rn00562332_m1	monocarboxylate transporter 1	Scl16a1
Nppa	Rn00561661_m1	natriuretic peptide precursor type A	ANF, ANP, Pnd, RATANF
Pcgf1	Rn01425394_g1	polycomb group ring finger 1	Nspc1
Pedf	Rn00709999_m1	pigment epithelium-derived factor	Serpinf1, Dmrs91
Rt1-dmb	Rn01429041_m1	RT1 class II, locus DMb	RT1-DMb, T1.DMb, RT1.Mb
Rt1-dra	Rn01427980_m1	RT1 class II, locus Da	H2-Ea, RT1-u
Rt1-drb1	Rn01429350_m1	RT1 class II, locus Db	RT1-Db, RT1-Db1n
Slc6a11	Rn00577664_m1	solute carrier family 6 (neurotransmitter transporter, GABA), member 11	Gat3, Gabt4
Stat3	Rn00562562_m1	signal transducer and activator of transcription 3	MGC93551
Timp1	Rn00587558_m1	tissue inhibitor of metalloproteinase 1	TIMP-1, Timp
Tnfrsf12a	Rn00710373_m1	tumor necrosis factor receptor superfamily, member 12a	Fn14, MGC72653